Design of a Light-Controlled Dual-Band Magnetic Resonant Wireless Power Transfer System

Ngoc Anh Nguyen
School of Electrical and Electronic Engineering, Hanoi University of Industry, Hanoi, Vietnam
nguyenngocanh@haui.edu.vn

Xuan Thanh Pham
School of Electrical and Electronic Engineering, Hanoi University of Industry, Hanoi, Vietnam
thanhpx@haui.edu.vn

Kim Hoan Vu
School of Electrical and Electronic Engineering, Hanoi University of Industry, Hanoi, Vietnam
vukimhoan9a@gmail.com

Thi Thuy Tien Tran
School of Electrical and Electronic Engineering, Hanoi University of Industry, Hanoi, Vietnam
thuytienthao123@gmail.com

Manh Kha Hoang
School of Electrical and Electronic Engineering, Hanoi University of Industry, Hanoi, Vietnam
khahoang@haui.edu.vn

Thanh Son Pham
School of Electrical and Electronic Engineering, Hanoi University of Industry, Hanoi, Vietnam
sonpt@haui.edu.vn (corresponding author)

Received: 6 April 2025 | Revised: 28 May 2025 | Accepted: 1 June 2025

 DOI: https://doi.org/10.48084/etasr.11325

ABSTRACT

Wireless Power Transfer (WPT) is an emerging technology that enables the transmission of electrical energy from a source to receiving devices without the necessity of physical conductors. This paper presents a Magnetic Resonant Wireless Power Transfer (MR-WPT) system with remote control capability using light. Light at a wavelength of 650 nm is employed to activate a photodiode placed on both the transmitter and receiver of the MR-WPT system. Depending on the active and inactive states of the incident light, the transmitter and receiver operate at different frequencies through a frequency control circuit embedded in the backside of resonators. This control circuit allows the MR-WPT system to function at two frequency bands, 13.0 MHz and 13.56 MHz, corresponding to the presence or absence of incident light, respectively. Simulations have been conducted to verify and elucidate the energy transfer mechanism and switching capability of the proposed MR-WPT system. Measurements indicate that at a transmission distance of 50 mm, the MR-WPT system achieves transmission coefficients of 0.74 at 13.0 MHz and 0.75 at 13.56 MHz. The results demonstrate that the MR-WPT system can operate efficiently with high performance across two different frequency bands, featuring a flexible remote control enabled by light.

Keywords-dual-band wireless power transfer; light controller; controlling; reconfigurable

I. INTRODUCTION

Since Nikola Tesla proposed the concept of Wireless Power Transfer (WPT) in the early 1900s, this technology has garnered significant attention worldwide [1]. Tesla envisioned a future where electrical energy could be transmitted wirelessly to various locations. Unfortunately, his project was discontinued due to resource constraints at the time. Throughout the 20th century, WPT was studied sporadically. However, in recent years, with the rapid advancement of technology and the exponential increase in the number of mobile devices, WPT has emerged as a critical solution [2]. WPT holds potential applications in various fields, such as wireless charging systems for electric vehicles, mobile phones, and other handheld devices [3, 4]. Additionally, extensive research on WPT is being conducted for applications in areas like biomedical implant technology and Autonomous Underwater Vehicles (AUVs) [5, 6].

Research on WPT in modern commercial applications primarily relies on two main methods: inductive coupling and magnetic resonance coupling [7, 8]. The earlier-developed inductive coupling technology enables high-efficiency wireless power transfer over short distances, typically ranging from millimeters to centimeters [9]. In contrast, magnetic resonance coupling, which has been developed more recently, allows power transfer over longer distances [10]. This makes it highly promising for applications requiring transmission distances of several centimeters or even meters. Moreover, in challenging transmission environments, magnetic resonance coupling is considered a more viable candidate compared to inductive coupling [11-15].

In conventional configurations, WPT systems typically operate at a fixed frequency due to the structure of resonant coils and externally attached capacitors, whose values cannot be adjusted [16]. To enhance the applicability of WPT, many studies have focused on controlling the operating frequency of the system [17, 18]. Some research has explored WPT systems with dual-frequency bands. Operating at multiple flexible frequency bands can enable WPT systems to function in various modes tailored to specific applications while also reducing interference among electronic devices [19-21]. Furthermore, in many cases where WPT systems operate in specialized environments, such as hazardous or inaccessible terrains, remote operation becomes a critical requirement. Consequently, the demand for a WPT system configuration capable of remote control to expand its range of applications is an important issue that warrants attention.

This paper explores a new method for controlling Magnetic Resonant Wireless Power Transmission (MR-WPT) systems. The proposal focuses on light-based remote control of resonant coils. The proposed design can achieve two resonant frequencies, allowing for flexible reconfiguration without compromising performance. We designed the MR-WPT system to operate at the 13.56 MHz frequency band in the absence of light impact and at the 13.0 MHz frequency band when remotely activated by light. The simulation and experimental results of transfer efficiency depending on resonant frequency have demonstrated the feasibility of the proposed MR-WPT system.

II. DESIGN AND ANALYSIS OF LIGHT–CONTROLLED MR-WPT SYSTEM

The remote control of electrical and electronic systems offers significant convenience and expands the potential applications of such devices. Figure 1 presents an MR-WPT system that can be operated using a red semiconductor laser with a wavelength of 650 nm. This MR-WPT system features a fundamental configuration consisting of four coils: source loop, transmitter resonator (Tx), receiver resonator (Rx), and receiver loop. The Tx and Rx resonators consist of a copper spiral coil with five turns fabricated on an FR-4 substrate. This classical coil design has been widely employed in the development of various WPT systems in previous studies [16]. The system is designed to operate at two frequency bands, 13.0 MHz and 13.56 MHz, corresponding to two scenarios: with and without laser illumination. With this configuration, the system can be easily controlled remotely via the laser light source to switch its operational mode from active to inactive or to toggle the working frequency between 13.0 MHz and 13.56 MHz, and vice versa.

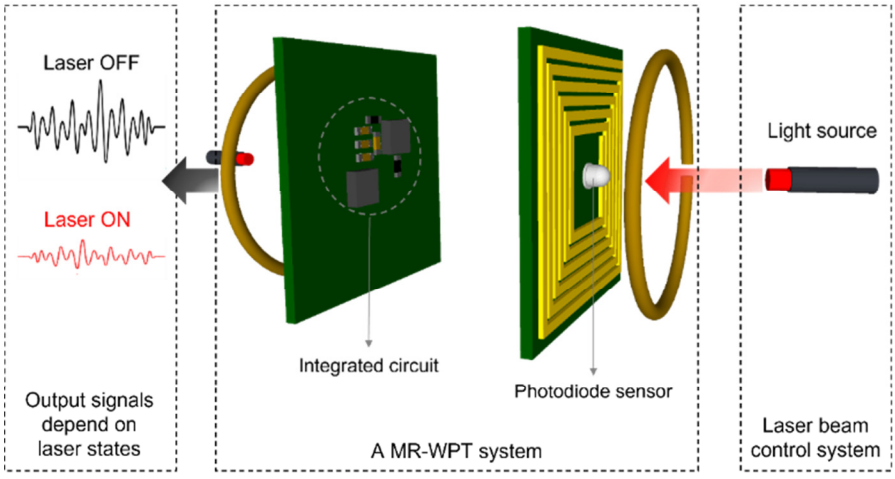

Fig. 1. Light-controlled MR-WPT system, with active (ON) and inactive (OFF) states of the laser beam.

The equivalent circuit model of the spiral coil and embedded circuit of the Tx and Rx resonators is shown in Figure 2. The coil can be modeled using components such as self-inductance (L_s), self-capacitance (C_s), and self-resistance (R_s). The natural resonance frequency of this coil is relatively high, reaching up to 116 MHz, which is unsuitable for WPT applications. Therefore, an external capacitor (C_0) is added to lower the operating frequency of the spiral coil. To control the operation of the Tx and Rx resonators, a varactor diode 1SV304TPH3F (C_v) is utilized, whose capacitance can be adjusted from 18 to 10 pF by applying a voltage in the range of 1 to 3 V. The voltage applied to the varactor diode C_v was regulated using an electrical circuit that includes a photodiode (D_1) capable of switching when exposed to light and a resistor R_1. To activate the photodiode, a red laser diode with a wavelength of 650 nm was used as the light source.

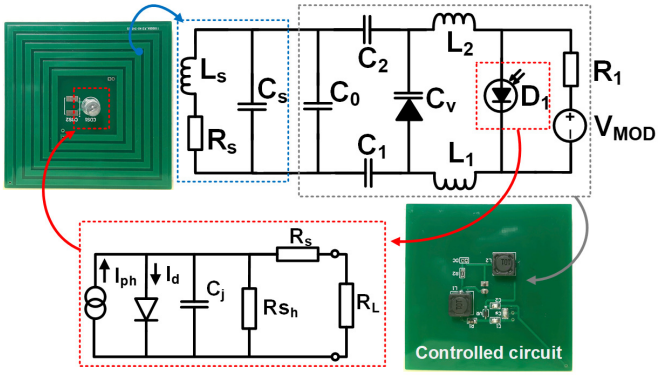

Fig. 2. Equivalent circuit of a resonator with the controlled circuit.

When the photodiode functions as a light-dependent resistor within the circuit, the total resistance varies based on the lighting conditions. The photodiode can be characterized by shunt resistance (Rs_h), series resistance (R_s), and junction capacitance (C_j). The shunt resistance, used to evaluate the noise current in a photodiode under no bias conditions (photovoltaic mode), is expected to exhibit a very high value, typically ranging from 10 to 1000 MΩ. The series resistance, which accounts for the combined resistance of the contacts and the undepleted material, can be described by the following formula [22]:

$$R_s = \frac{(W_s - W_d)\rho}{A} + R_c \quad (1)$$

where W_s represents the thickness of the substrate, W_d is the width of the depleted region, A denotes the diffused area of the photodiode junction, ρ is the resistivity of the substrate, and R_c is the contact resistance. When light is incident on the photodiode, the resistivity (ρ) decreases, leading to a reduction in the overall resistance of the photodiode. This resistance (R_s) typically ranges from 10 to 1000 Ω. In the actual experimental setup, we utilized the Silicon PIN Photodiode SFH 213. The measured resistance of the photodiode is 200 Ω and 10 MΩ, corresponding to the presence and absence of red laser excitation.

In order to make the system operate at two distinct frequencies, two ends of the spiral are connected to the back panel through a circuit on the back side of the structure. This circuit is responsible for changing the total capacity so that the resonant operating frequency can be controlled.

The total capacitance of the coil with an embedded circuit can be calculated:

$$C_{total} = C_S + C_0 + \left(\frac{1}{C_1} + \frac{1}{C_2} + \frac{1}{C_V}\right)^{-1} \quad (2)$$

Here, C_1 and C_2 are external capacitors to prevent the Direct Current (DC) from V_{MOD} flowing into the spiral coil. Conversely, the two inductors L_1 and L_2 are used to block the Alternating Current (AC) from the coil to the photodiode and the source V_{MOD}.

Figure 3(a) illustrates the frequency response of the resonator under two conditions: with the laser diode active and inactive. All the circuit component values are presented in Table I. It can be observed that under normal conditions, when no light is incident on the resonator, the V_{MOD} source supplies a voltage of 3 V to the varactor diode, resulting in a capacitance value of 10 pF. At this capacitance, the resonator resonates at a frequency of 13.56 MHz (black curve). When the laser diode is activated, the light incident on the photodiode causes it to conduct, leading to a drop in the voltage supplied to the varactor diode to 1 V, corresponding to a capacitance value of 18 pF. This shift in capacitance causes the resonator's resonance frequency to shift to a lower frequency, at 13.0 MHz (red curve).

Figure 3(b) shows the phase response of the resonator under the same conditions as Figure 3(a). In the absence of illumination, the phase response of the resonator exhibits a phase inversion at a frequency of 13.56 MHz. Conversely, when illuminated by the laser light and activating the photodiode, the phase inversion points red-shifts to a frequency of 13.0 MHz. These results are in excellent agreement with the theoretical analyses presented above.

TABLE I. CIRCUIT COMPONENT VALUES USED IN THE MR-WPT SYSTEM

Component	Value
R_s (Ω)	0.68
L_s (μH)	1.48
C_s (pF)	1.5
C_0 (pF)	82
C_1 (nF)	1
C_2 (nF)	1
C_v (pF)	10, 18
L_1 (μH)	200
L_2 (μH)	200
R_{D1} (Ω)	200 Ω-10 MΩ
R_1 (Ω)	400 Ω
V_{MOD} (V)	3

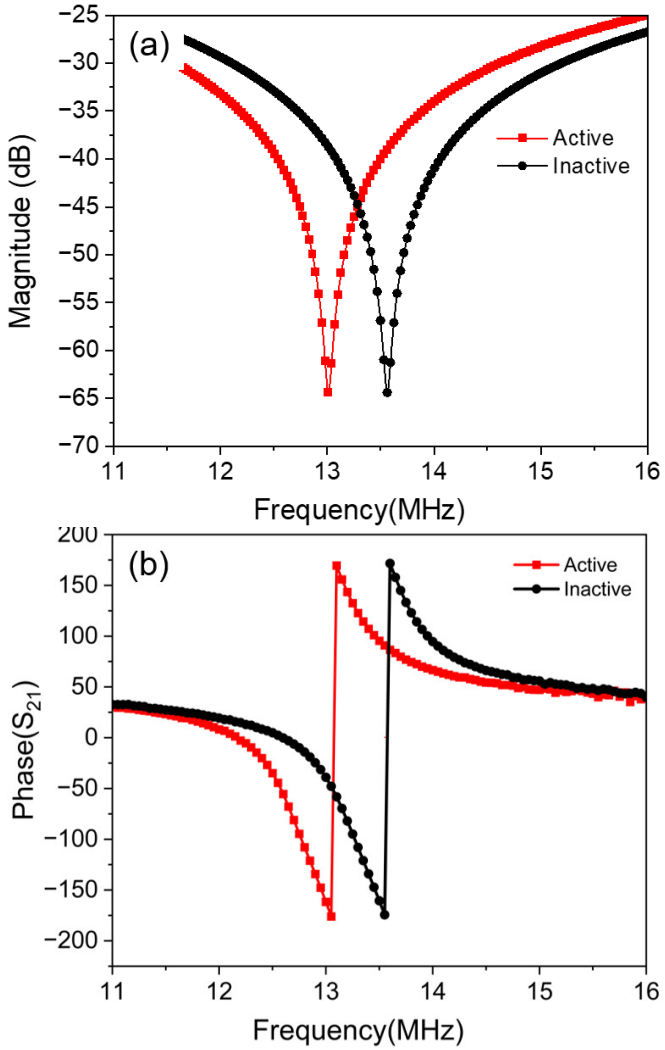

Fig. 3. (a) Simulated frequency response of the resonator in the active and inactive modes, (b) phase shift of S_{21}.

To evaluate the performance of the MR-WPT system operating at two different frequencies, 13.0 MHz and 13.56 MHz, simulations were conducted using the CST Studio Suite software to observe the field distribution around the system. Figure 4 illustrates the magnetic field distribution around the MR-WPT system, with system parameters listed in Table II. The results indicate that, in the case where both the transmitter (Tx) and receiver (Rx) are in an inactive state (Figures 4(a) and 4(c)), the MR-WPT system exhibits a strong magnetic field at both Tx and Rx at a frequency of 13.56 MHz. In contrast, at 13.0 MHz, the magnetic field intensity is weak at both Tx and Rx, with the field at Rx being almost negligible and equivalent to the free space. Conversely, in the active state (Figures 4(b) and 4(d)), the field intensities observed at 13.56 MHz and 13.0 MHz are reversed compared to the inactive state. In cases where only Tx or Rx is active (Figures 4(e-h)), it was observed that at 13.56 MHz, the magnetic field at both Tx and Rx is very weak, whereas at 13.0 MHz, the magnetic field intensity at Rx is stronger compared to that at 13.56 MHz.

This implies that the MR-WPT system will have a transmission peak at a frequency close to 13.0 MHz when only one of the two resonators, either Tx or Rx, is active. However, when only Tx or Rx is active, the transmission efficiency is significantly lower compared to the cases where both Tx and Rx are either active or inactive simultaneously.

TABLE II. TECHNICAL SPECIFICATIONS OF THE MR-WPT SYSTEM

Specification	Source loop	Load loop	Tx resonator	Rx resonator
R (Ω)	0.06	0.06	0.68	0.68
L (μH)	0.088	0.088	1.48	1.48
Number of turns	1	1	5	5
Inner diameter (mm)	42.5	42.5	20	20
Outer diameter (mm)	45	45	50	50
Copper thickness (mm)	–	–	0.035	0.035
Strip width (mm)	–	–	2	2
Spacing between strips (mm)	–	–	1	1
Resonant frequency (MHz)	–	–	13.56	13.56

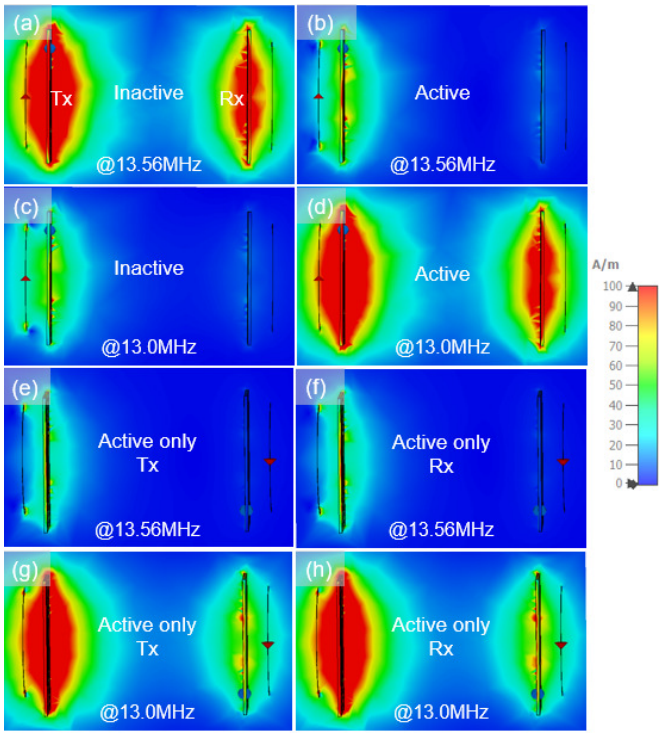

Fig. 4. Magnetic field distribution of the MR-WPT system at 13.0 MHz and 13.56 MHz for several configurations: (a) Tx & Rx inactive at 13.56 MHz, (b) Tx & Rx active at 13.56 MHz, (c) Tx & Rx inactive at 13.0 MHz, (d) Tx & Rx active at 13.0 MHz, and (e-h) only Tx or Rx active at either 13.56 MHz or 13.0 MHz.

III. RESULTS AND DISCUSSION

Following a comprehensive analysis of the effects of the light-controlled dual-band WPT system, we proceeded to fabricate the MR-WPT system and conducted empirical measurements, as illustrated in Figure. 5. The MR-WPT system was constructed based on the schematic presented in Figure 1.

To evaluate the performance of the fabricated MR-WPT system, we utilized a Vector Network Analyzer (VNA) model KEYSIGHT P3975A. Prior to the measurements, the VNA was calibrated using the 2-port calibration Short-Open-Load-Through (SOLT) method. The two loop antennas of the system were connected to the two ports of the VNA to measure the reflection and transmission coefficients. The fabricated MR-WPT system was measured at a fixed distance of d_{23} = 50 mm. The values of d_{12} and d_{34} were adjusted to ensure that the S_{11} parameter was less than -10 dB to minimize impedance mismatch. A DC power supply was employed to provide reverse bias voltage for the varactor diode and to power the laser diode for operation.

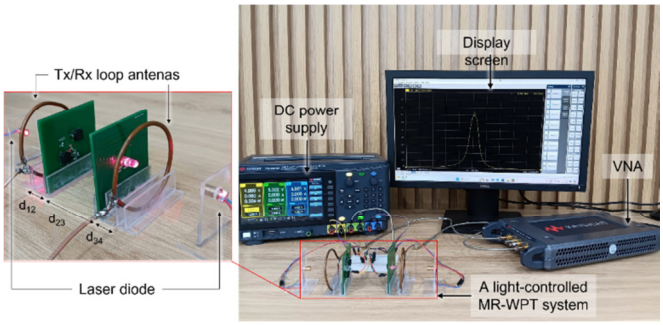

Fig. 5. Experiment setup for the proposed MR-WPT system.

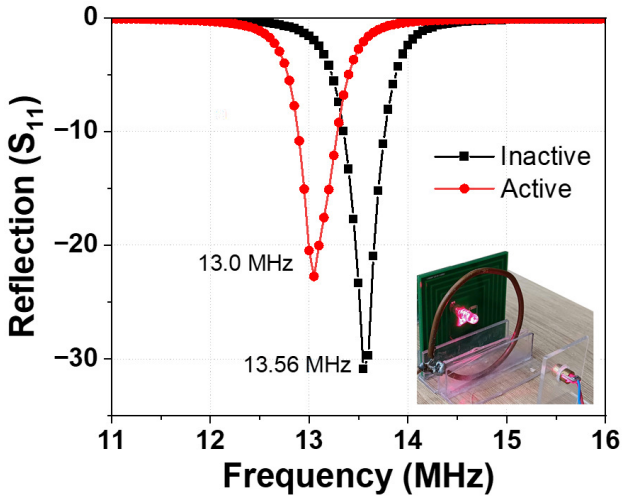

Fig. 6. Reflection coefficient S_{11} of the MR-WPT system under both inactive and active light conditions.

To investigate the operation of the resonator, we fabricated the loop antenna and resonators with parameters as presented in Table II. Due to the symmetrical nature of the MR-WPT system, both the Tx and Rx resonators share identical dimensions and parameters. They were fabricated using copper on an FR-4 substrate with a thickness of 1.2 mm. The self-inductance and self-resistance values of the resonators are also measured and listed in Table II. Figure 6 presents the measured reflection response of the resonators under both illuminated and non-illuminated conditions. The results obtained align well with the theoretical analyses discussed in the previous sections. Specifically, the results indicate that the Tx and Rx resonators have a resonant frequency of 13.56 MHz in the absence of illumination, with a reflection coefficient of S_{11} = -32 dB, and a resonant frequency of 13.0 MHz under illumination, with a reflection coefficient of S_{11} = -23 dB.

The quality factor (Q-factor) of the resonator is a critical parameter that significantly affects the performance of the WPT system. When the MR-WPT system operates at two different frequencies, variations in the Q-factor may occur. Figure 7 illustrates the Q-factor of the resonator at various frequencies. It can be observed that the resonator achieves a maximum Q-factor of 380 at 52 MHz. This maximum Q-factor is dependent on the size and configuration of the resonator. However, at the two operating frequencies of the MR-WPT system, ranging from 13.0 to 13.56 MHz, the Q-factor exhibits negligible variation, reaching values of 245 and 248, respectively. This indicates that the MR-WPT efficiency at 13.56 MHz will be slightly higher than at 13.0 MHz; however, the difference is insignificant.

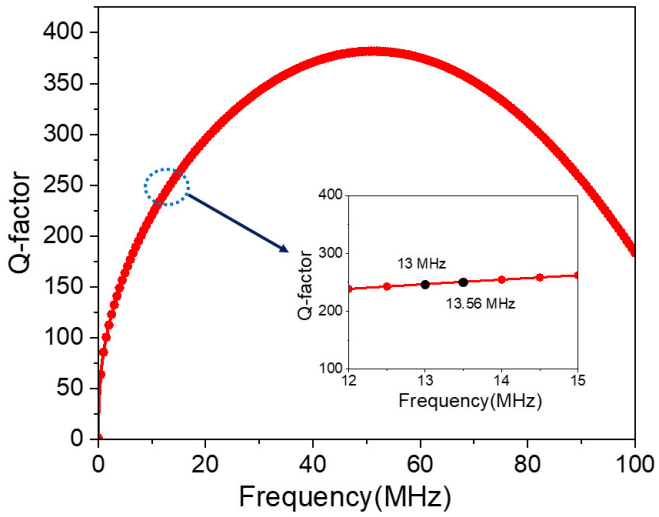

Fig. 7. Q-factor of the resonator at two frequencies: 13.0 MHz and 13.56 MHz.

Figure 8 shows the measurement results of the system with the distance between the two resonators surveyed from 5 mm to 100 mm in the case without the light. When the transmission distance is d_{23} = 50 mm, the system works in critical coupling mode with a transmission coefficient of 0.75. If d_{23} > 50 mm, the MR-WPT system operates in the under-coupling region, and the coupling between Tx and Rx resonators quickly decreases, leading to reduced WPT performance. If d_{23} < 50 mm, the MR-WPT system operates in the over-coupling region, and it suffers from the frequency splitting effect. Then, because the coupling is too strong, the resonance is split into two upper and lower frequencies, which is why the transmission efficiency at the original resonant frequency (13.56 MHz) is degraded.

Figure 9 presents the transmission coefficient results of the MR-WPT system under four different configurations. The first case corresponds to the original MR-WPT system, where no light illumination is applied to the photodiode. Under normal

conditions, the MR-WPT system achieves a transmission peak at 13.56 MHz, which is the resonant frequency of the two resonant coils. In this scenario, the transmission coefficient reaches a value of 0.75, as shown in Figure 9(a). In the second case, both the Tx and Rx are illuminated. Due to the resonance frequencies of both resonators shifting to 13.0 MHz, the transmission peak is observed at this frequency. Figure 9(b) demonstrates that the peak transmission in this case is 0.74, comparable to the scenario without laser illumination. The slightly lower transmission coefficient is attributed to the reduced Q-factor of the resonators at 13.0 MHz compared to 13.56 MHz. Meanwhile, at 13.56 MHz, the transmission coefficient significantly decreases to only 0.15. In the case where only one resonator is illuminated, the resonance frequencies of the two coils are detuned to 13.0 MHz and 13.56 MHz, respectively. This results in a trade-off frequency for the highest transmission coefficient occurring between these two frequencies. Due to the symmetrical nature of the MR-WPT system in this study, when either the Tx (Figure 9(c)) or the Rx (Figure 9(d)) is illuminated, the transmission spectrum peak consistently occurs at 13.25 MHz, with respective values of 0.21 and 0.20. The appearance of the transmission peak at this frequency is attributed to the overlap of two resonance peaks at 13.0 MHz and 13.56 MHz. The slight difference between the peak transmission values in these two cases can be explained by measurement errors and variations in the experimental setup.

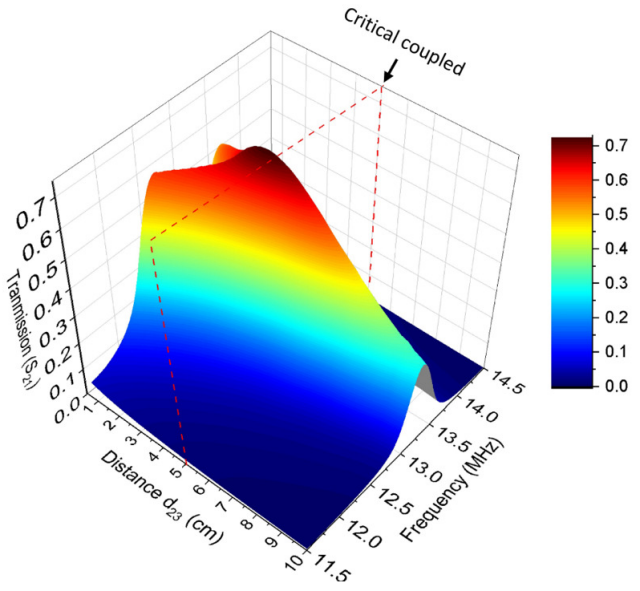

Fig. 8. Transmission coefficient of the original MR-WPT system as a function of distance. The transmission distance d_{23} has been adjusted to achieve the optimal position prior to activation and inactivation.

The measurement results demonstrate consistency with the simulation results shown in Figure 4. The fabricated MR-WPT system has the capability of remote control via laser diode light. The integrated circuit presented in Figure 2 performed well, exhibiting low loss, as evidenced by the high transmission coefficient of the measured MR-WPT system. Although MR-WPT systems have been extensively studied, designing a system with remote control capability and operation at two distinct frequency bands remains significant and contributes to the development of MR-WPT systems operating under various conditions.

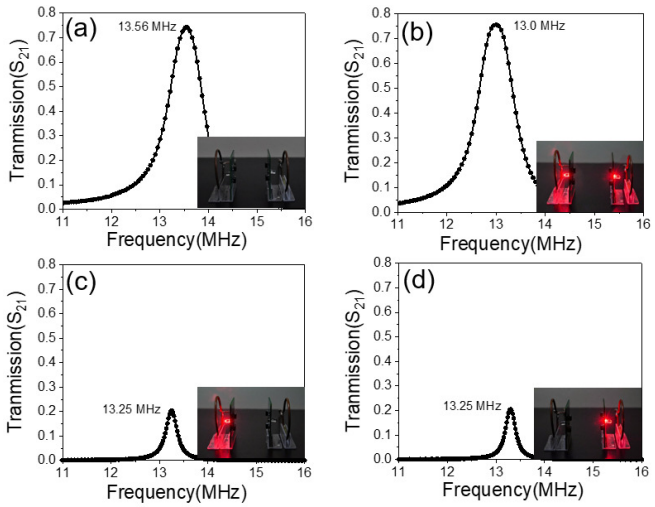

Fig. 9. Transmission coefficient of the MR-WPT system in four different configurations: (a) Tx and Rx are not illuminated, (b) Tx and Rx are illuminated, (c) Tx is illuminated, and (d) Rx is illuminated.

IV. CONCLUSION

This paper presents an Magnetic Resonant Wireless Power Transfer (MR-WPT) system capable of controlling its operating frequency through illumination from a laser diode. A red-light laser diode with a wavelength of 650 nm is utilized to adjust the operating frequency of the MR-WPT system via a control circuit employing a varactor diode. The results obtained from illuminating and non-illuminating the photodiode at resonators demonstrate that the MR-WPT system can switch between two frequencies, 13.0 MHz and 13.56 MHz. The transmission coefficients in both cases are high and fairly similar, with values of S_{21} = 0.74 and S_{21} = 0.75, respectively. Furthermore, simulations were conducted to analyze the magnetic field distribution around the MR-WPT system under various conditions. These simulations demonstrated a high degree of agreement with the experimental measurements, validating the model's accuracy and reliability. The MR-WPT system, which is controlled by light and has two distinct frequency operating bands, was first proposed and subsequently tested in experiments that proved its efficacy. The findings of this study can be applied to the design of flexible MR-WPT systems capable of remote frequency switching and operation across multiple frequency bands. This, in turn, enhances the controllability, adaptability, and potential applications of Wireless Power Transfer (WPT) technology.

ACKNOWLEDGMENT

The authors would like to acknowledge the support for this project from the Hanoi University of Industry Research Fund under grant number 52-2024-RD/HD-DHCN.

REFERENCES

[1] N. Tesla, "Apparatus for transmitting electrical energy," US1119732A, Dec. 01, 1914.

[2] J. M. Stankiewicz, A. Steckiewicz, and A. Choroszucho, "Analysis of Simultaneous WPT in Ultra-Low-Power Systems with Multiple Resonating Planar Coils," *Energies*, vol. 16, no. 12, Jun. 2023, Art. no. 4597, https://doi.org/10.3390/en16124597.

[3] B. A. Rayan, U. Subramaniam, and S. Balamurugan, "Wireless Power Transfer in Electric Vehicles: A Review on Compensation Topologies, Coil Structures, and Safety Aspects," *Energies*, vol. 16, no. 7, Apr. 2023, Art. no. 3084, https://doi.org/10.3390/en16073084.

[4] N. T. Diep, T. D. Hiep, and N. K. Trung, "Constant Current Charging and Transfer Efficiency Improvements for a Dynamic Wireless Charging System," *Engineering, Technology & Applied Science Research*, vol. 13, no. 6, pp. 12320–12326, Dec. 2023, https://doi.org/10.48084/etasr.6315.

[5] D. Shan, H. Wang, K. Cao, and J. Zhang, "Wireless power transfer system with enhanced efficiency by using frequency reconfigurable metamaterial," *Scientific Reports*, vol. 12, no. 1, Jan. 2022, Art. no. 331, https://doi.org/10.1038/s41598-021-03570-8.

[6] N. H. Solouma, H. B. Kassahun, A. S. Alsharafi, A. Syed, M. R. Gardner, and S. S. Alsharafi, "An Efficient Design of Inductive Transmitter and Receiver Coils for Wireless Power Transmission," *Electronics*, vol. 12, no. 3, Feb. 2023, Art. no. 564, https://doi.org/10.3390/electronics12030564.

[7] Y. Sun and S. Beeby, "Simulation of 2-Coil and 4-Coil Magnetic Resonance Wearable WPT Systems," *Proceedings*, vol. 68, no. 1, Jan. 2021, Art. no. 13, https://doi.org/10.3390/proceedings2021068013.

[8] C. Degen, "Inductive coupling for wireless power transfer and near-field communication," *EURASIP Journal on Wireless Communications and Networking*, vol. 2021, no. 1, May 2021, Art. no. 121, https://doi.org/10.1186/s13638-021-01994-4.

[9] M. Rehman *et al.*, "A Review of Inductive Power Transfer: Emphasis on Performance Parameters, Compensation Topologies and Coil Design Aspects," *IEEE Access*, vol. 11, pp. 144978–145010, 2023, https://doi.org/10.1109/ACCESS.2023.3344041.

[10] H. N. Bui, T. S. Pham, V. Ngo, and J.-W. Lee, "Investigation of various cavity configurations for metamaterial-enhanced field-localizing wireless power transfer," *Journal of Applied Physics*, vol. 122, no. 9, Sep. 2017, Art. no. 093102, https://doi.org/10.1063/1.5001130.

[11] F. Bennia, A. Boudouda, and F. Nafa, "Optimal design of wireless power transfer coils for biomedical implants using machine learning and meta-heuristic algorithms," *Electrical Engineering*, vol. 106, no. 5, pp. 5869–5884, Oct. 2024, https://doi.org/10.1007/s00202-024-02345-4.

[12] R. Hasaba, K. Okamoto, S. Kawata, K. Eguchi, and Y. Koyanagi, "Magnetic Resonance Wireless Power Transfer Over 10 m With Multiple Coils Immersed in Seawater," *IEEE Transactions on Microwave Theory and Techniques*, vol. 67, no. 11, pp. 4505–4513, Nov. 2019, https://doi.org/10.1109/TMTT.2019.2928291.

[13] A. Alipour *et al.*, "Improvement of magnetic resonance imaging using a wireless radiofrequency resonator array," *Scientific Reports*, vol. 11, no. 1, Nov. 2021, Art. no. 23034, https://doi.org/10.1038/s41598-021-02533-3.

[14] W. Zhou, S. Sandeep, P. Wu, P. Yang, W. Yu, and S. Y. Huang, "A Wideband Strongly Coupled Magnetic Resonance Wireless Power Transfer System and Its Circuit Analysis," *IEEE Microwave and Wireless Components Letters*, vol. 28, no. 12, pp. 1152–1154, Dec. 2018, https://doi.org/10.1109/LMWC.2018.2876767.

[15] H. Hwang, J. Moon, B. Lee, C. Jeong, and S. Kim, "An analysis of magnetic resonance coupling effects on wireless power transfer by coil inductance and placement," *IEEE Transactions on Consumer Electronics*, vol. 60, no. 2, pp. 203–209, May 2014, https://doi.org/10.1109/TCE.2014.6851995.

[16] M. K. Hoang, X. T. Kieu, X. T. Pham, T. K. Vu, and T. S. Pham, "A Design of Magnetic Resonant Wireless Power Transfer System using Flexible Resonator Coils," *Journal of Magnetics*, vol. 28, no. 3, pp. 323–330, Sep. 2023, https://doi.org/10.4283/JMAG.2023.28.3.323.

[17] J.-J. Kao, C.-L. Lin, and J. Yang, "Adaptive Wireless Power Transfer System With Relay Transmission and Communication," *IEEE Transactions on Power Electronics*, vol. 38, no. 3, pp. 4110–4123, Mar. 2023, https://doi.org/10.1109/TPEL.2022.3218368.

[18] X. Jiang, R. K. Pokharel, A. Barakat, and K. Yoshitomi, "A multimode metamaterial for a compact and robust dualband wireless power transfer system," *Scientific Reports*, vol. 11, no. 1, Nov. 2021, Art. no. 22125, https://doi.org/10.1038/s41598-021-01677-6.

[19] A. Jabbari, C. Simovski, and M. Sharifian Mazraeh Mollaei, "Tunable Dual-Band High-Impedance Coil for Wireless Power Transfer Applications," *IEEE Transactions on Antennas and Propagation*, vol. 71, no. 12, pp. 9467–9476, Dec. 2023, https://doi.org/10.1109/TAP.2023.3318837.

[20] B. Garnier, P. Mariage, F. Rault, C. Cochrane, and V. Koncar, "Textile dual-band NFC-A4WP (13.56–6.78 MHz) combiner for wireless energy and data transmission for connected clothing," *Scientific Reports*, vol. 13, no. 1, Apr. 2023, Art. no. 5613, https://doi.org/10.1038/s41598-023-31832-0.

[21] A. Fereshtian and J. Ghalibafan, "Impedance matching and efficiency improvement of a dual-band wireless power transfer system using variable inductance and coupling method," *AEU - International Journal of Electronics and Communications*, vol. 116, Mar. 2020, Art. no. 153085, https://doi.org/10.1016/j.aeue.2020.153085.

[22] V. D. B. Bonifacio and R. F. Pires, "Photodiodes: Principles and recent advances," *Materials NanoScience*, vol. 6, no. 2, pp. 38–46, Jul. 2019.